Journal of Alloys and Compounds 509 (2011) 4797–4804

Contents lists available at ScienceDirect

Journal of Alloys and Compounds

journal homepage: www.elsevier.com/locate/jallcom

Optimization of processing conditions and characterization investigations of ceramic injection molded and sintered ZrO_2/WC composites

N. Ünal[a,b,*], F. Kern[a], M.L. Öveçoğlu[b], R. Gadow[a]

[a] Universität Stuttgart, Institut für Fertigungstechnologie Keramischer Bauteile (IFKB), Allmandring 7b, 70569 Stuttgart, Germany
[b] Particulate Materials Laboratories, Department of Metallurgical and Materials Engineering, Faculty of Chemical-Metallurgical Engineering, Istanbul Technical University, ITU Ayazaga Kampusu Maslak, 34469 Istanbul, Turkey

ARTICLE INFO

Article history:
Received 19 November 2010
Received in revised form 18 January 2011
Accepted 30 January 2011
Available online 23 February 2011

Keywords:
Ceramic matrix composites
Particle size distribution
Wear/wear resistance
Mechanical properties
Microstructure

ABSTRACT

In this investigation, 3 mol% Y_2O_3 stabilized ZrO_2-based composites reinforced with 10 vol.%, 20 vol.% and 40 vol.% WC (named as 3Y-TZP/10WC, 3Y-TZP/20WC and 3Y-TZP/40WC) were fabricated by using injection molding and sintering. Mechanical properties of these composites varied due to WC addition and dwelling time. Density, strength and toughness decreased with shorter dwelling time and increasing WC content however a significant enhancement in fracture toughness was obtained by 3Y-TZP/20WC composite which had 9.2 MPa $m^{1/2}$ toughness. Severe unlubricated wear tests which were performed under 55 N normal load and 45 km sliding distance showed that 3Y-TZP/20WC composite had the lowest wear rate and wear volume values which are 2×10^{-8} $mm^3/(N\,m^{-1})$ and 0.05 mm^3, respectively.

1. Introduction

Ceramic injection molding (CIM) is an innovative forming technique in manufacturing a range of components, including those with a high geometric complexity and it offers an economic solution for difficult production problems. CIM has become a highly attractive process for the production of geometrically complex ceramic parts in large scale manufacturing [1]. The inherent hardness of ceramics infers that manufacturing complex shaped ceramic components by standard machining processes can be expensive. CIM offers an economic solution for delivering repeatable, ultra high precision ceramic components. The injection molding of ceramics is a new and innovative process that provides cost effective solutions for design engineers requiring complex, repeatable ceramic components [1–3].

ZrO_2-based ceramics have been demonstrated to be the strongest and toughest oxide yet produced. The excellent properties are attributed to the stress-induced phase transformation from tetragonal to monoclinic ZrO_2 [4,5]. However, for tribological applications, the limited hardness is a big handicap. Therefore to improve the modest hardness of ZrO_2, refractory hard phases such as WC, TaC and TiC have been dispersed into the stabilized-ZrO_2 matrix [5–10]. Hot pressing experiments have demonstrated that WC secondary hard phase addition enhanced the hardness of ZrO_2 matrix while preserving its high toughness [4,10].

Several research investigations have been focused on the production of ZrO_2/WC composites by hot pressing and spark plasma sintering (SPS) [4–6,11–14] and pressureless sintering techniques following cold compaction [15–17]. Currently, although there have been several investigations based on the injection molding of ZrO_2; ZrO_2-based matrix ceramics have been mostly produced by hot pressing technique to obtain high mechanical properties with the help of applying pressure during sintering. As an alternative processing route, the present study has shown that injection molding is a promising production technique in the fabrication of yttria stabilized ZrO_2/WC composites. In the present study, various amounts of WC refractory carbide reinforced yttria stabilized ZrO_2 matrix composites were produced using CIM technique prior to pressureless sintering. The challenges in this study were to determine the binder amount, debinding schedule and sintering conditions due to longer sintering times and temperatures compared with hot pressing. Many different composite compositions, injection molding parameters and characterization techniques were used to optimize the production variables. Furthermore, the mechanical effect of bimodal particle size distribution of the secondly distributed WC phase was observed and reported.

2. Experimental procedure

To optimize the stabilizer amount and WC fraction, commercial coarse-WC powders in the amounts varying between 10 vol.% and 40 vol.% were dispersed in yttria

* Corresponding author at: Istanbul Technical University, Department of Metallurgical and Materials Engineering, Particulate Materials Laboratories, 34469 Istanbul, Turkey.
E-mail address: nil_unal@yahoo.com (N. Ünal).

0925-8388/$ – see front matter © 2011 Elsevier B.V. All rights reserved.
doi:10.1016/j.jallcom.2011.01.167

Table 1
The characteristics of the starting powders.

Powder material	Particle size (D_{50})	S_{BET} ($m^2\ g^{-1}$)	Supplier	Grade
Pure ZrO_2	560 nm[a]	15.90[b]	Tosoh	TZ-0
3Y-TZP	590 nm[a]	6.80[b]	Tosoh	TZ-3YS-E
Coarse-WC	1.49 μm[a]	0.93[a]	Alfa Aesar	WC
Fine-WC	184 nm[a]	1.64[a]	Milled	WC

[a] Measured data.
[b] Supplier's data.

stabilized ZrO_2 matrix. 2, 2.5 and 3 mol% yttria stabilized zirconia were prepared using suitable mixtures of commercial powders which were unstabilized ZrO_2 and 3 mol% yttria stabilized ZrO_2 (3Y-TZP). To obtain fine-WC powders, a high energy Spex™ mixer mill was used for 10 min with a WC/Co milling system. Mean particle size of the powders was determined by a Malvern™ Laser particle size analyzer. The properties of the powders are shown in Table 1.

Commercially available water-soluble (Licomont™ EK 583G) binder was used to prepare the feedstocks. Solid content was varied between 44 and 51 vol.% according to fine and coarse WC content in the composition. Feedstocks were mixed in a double sigma blade kneader (Hermann Linden™ Maschinenfabrik, Marienheide) with a twin screw extruder (Thermofisher™) unit at 120 °C followed by homogenization of granulated feedstocks in a twin screw extruder at 140 °C. Some extruded bars ($30 \times 3 \times 5$) were spared for optimizing sintering conditions. Following to homogenization, a capillary rheometer (Thermofisher™ Rheomex) unit was attached to the extruder and rheometer measurements were performed between 130 and 160 °C using a nozzle having a diameter (D) of 2.0 mm and length per diameter (l/d) of 15. Granulated feedstocks were injection molded into two different molds. Injection molding parameters which were optimized for the mold having plate and bar cavity is given in Table 2. The dimensions of the first molds were: 7 mm × 7 mm × 70 mm stick and a ring that has an outer diameter (Øi) of 19.9 mm, a wall thickness (b) of 4 mm and a height (h) of 3.4 mm. As a second mold system, a plate with the dimensions of 32 mm × 3 mm × 45 mm and an additional core which has a diameter of 0.3 mm and a bar cavity with the dimensions of 4 mm × 3 mm × 30 mm in the same mold were used. Produced parts were debinded firstly in distilled water at 60 °C for 24 h, followed by drying at the same temperature. Thermal debinding was carried out at 300 °C using a heating rate of 10 K/h for 12 h in air. After all debinding steps shape and weight differences were measured dimensionally. Hg-porosimetry measurements on the brown parts (after debinding) were carried out in a ThermoScientific Mercury Porosimeter PASCAL 440™ with a mercury surface tension of 480 dyn/cm and a contact angle of 141.3° in average to calculate the pore size distribution. Furthermore, DTA/TG investigations of the green and brown parts were conducted in a Netzsch™ DTA/DSC/TGA up to 1590 °C using a heating rate of 5 K/min. For the green parts (before debinding), DTA/TG measurements were carried out in air, and for the brown parts in argon (Ar) atmosphere.

To observe the sintering behavior of the debinded parts, dilatometer measurements were conducted in a Netzsch™ dilatometer up to 1590 °C using a heating rate of 5 K/min. On the basis of the dilatometry tests, sintering was performed at 1550 °C with 4 h and 6 h dwelling times, using a heating rate of 5 K/min. H_2 gas flowing conditions were employed up to 950 °C without any dwell followed by Ar gas flowing conditions up to the sintering temperatures and cooling down to the room temperature. Archimedes density measurements were done using ethanol on sintered samples followed by metallographical preparations for microstructural analyses. Scanning electron microscope (SEM) (Leo™ VP 438; operated at 15 kV) and X-ray diffraction (XRD) investigations of the sintered samples were carried out using Bruker™ D-8 Advance XRD (Cu Kα radiation, λ = 0.15418 nm) diffractometer at 40 kV and 40 mA settings in the 2θ range from 25° to 80°.

3 point bending tests using the DIN EN ISO 6872 standard [18] were carried out on five bending bars of each sample at room temperature to measure the flexural strengths. Young's modulus and Vickers microhardness values were analyzed using a Fischerscope™ HCU microhardness testing machine by applying 10 indentations under 100 g load for 10 s on each sample. Vickers hardness measurements were carried out with a 10 kg load for 10 s. Using the Niihara equation, fracture toughness values of the composites were calculated by the crack length measurements obtained with HV_{10} indentations [7]. Unlubricated reciprocating wear tests were performed using a pin-on-disc machine (Johann Fischer™ Aschaffenburg) with a 5 mm diameter tungsten carbide ball pin at the ambient temperature and at ambient humidity. The balls were renewed in each experiment. The normal load and sliding speed were 55 N and 0.07 m/s, respectively. For each test, a total of 45 km total sliding distance was performed on a 5 mm stroke. Friction force was monitored simultaneously using a force transducer. Surface profiles of the worn surfaces and the wear volume were acquired using profilometer (Mahr™ Perthometer PGK).

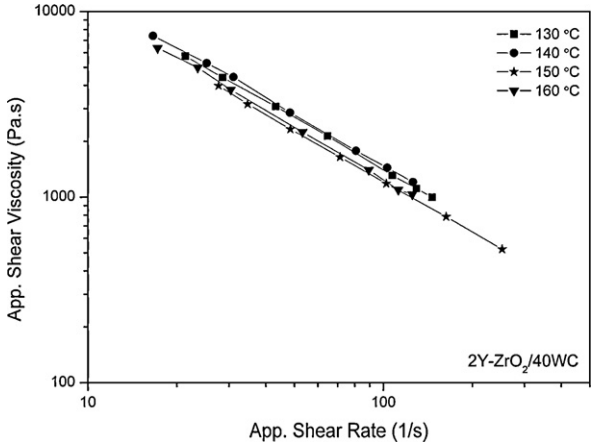

Fig. 1. Capillary rheometer measurements of the 2Y-TZP/40WC feedstocks at different temperatures.

3. Results and discussion

3.1. Optimization of injection molding and pre-sintering parameters

To observe the rheological behavior of the feedstocks, capillary rheology measurements on homogenized 2 mol% Y_2O_3 stabilized ZrO_2 matrix composites with 40 vol.% WC addition (2Y-TZP/40WC) were carried out using a nozzle with a $D = 2.0$ mm and $l/d = 15$ dimensions. Fig. 1 shows capillary rheometer measurement results (shear viscosity versus shear rate) taken at the temperatures of 130 °C, 140 °C, 150 °C and 160 °C, revealing viscosity lowered linearly with increasing shear rate up to 160 °C. At 160 °C, shear thinning behavior was observed until the shear rate reached to 100 s^{-1} but with increasing shear rate the viscosity stayed stable. For the measurements at 150 °C, the viscosity value even declined to 525 Pa s as the shear rate was 250 s^{-1}. Therefore, 150 °C was selected as suitable temperature for injection molding.

Table 2
Injection molding parameters of the feedstocks.

Molding variables	3Y-TZP/10WC	3Y-TZP/10WC (75% coarse)	3Y-TZP/20WC	3Y-TZP/40WC
Solid content (vol.%)	46	44	47	51
Mold temperature (°C)	65	65	65	60
Nozzle temperature (°C)	160	160	160	155
Injection speed ($cm^3\ s^{-1}$)	40	40	40	35
Injection pressure (bar)	1350	1350	1550	1600
Hold pressure (bar)	1400	1400	1400	1200
Cooling time (s)	20	20	20	20

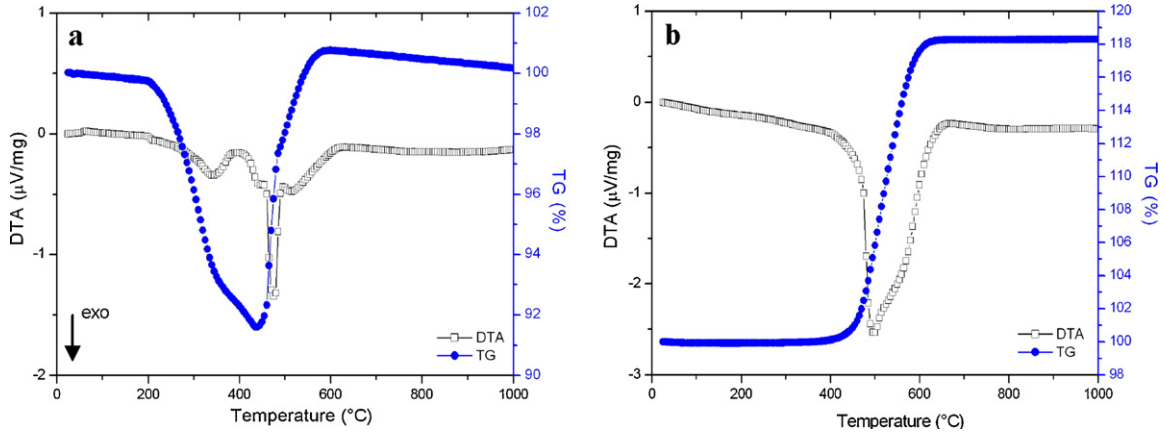

Fig. 2. DTA–TG graph of the (a) 3Y-TZP/40WC composite before water debinding and (b) DTA–TG graph of the starting WC powder.

Due to the pressure limit (100 bar) of the rheometer device, the viscosity at higher shear rates could not be measured. Similar flow behavior with increasing temperature was observed for other feedstocks. Consequently, it was observed that injection molding could be performed without problems at the plasticization temperature of 150 °C.

The samples were injection molded into two different molds with optimized injection parameters. Injection pressure was increased from 1350 bar to 1600 bar with increasing WC amount. General injection molding parameters of the WC added 3Y-TZP feedstocks are given in Table 2.

As seen in Table 2, when the system had 25 vol.% fine-WC powders, the binder amount was slightly getting higher. As the amount of WC phase in 3Y-TZP matrix increases, higher injection pressures and lower speed were needed, though it complicated processing. In addition, with higher WC amount, flow lines and jetting problems were observed.

Prior to debinding, DTA/TG measurements were carried out on extruded green samples under air to optimize the debinding conditions. Fig. 2a and b is the DTA/TG graphs of the 3Y-TZP/40WC composite and the starting WC powders, respectively. It is evident from Fig. 2 that the green bodies continuously lost weight starting from 200 °C until 490 °C. At 490 °C, oxidation took place and the parts gained weight. To observe oxidation, DTA/TG measurements were carried out with the same conditions on the WC powders. Oxidation rate reached its maximum at 498.2 °C, indicating that WC was oxidized to form WO_3. XRD investigations revealed the formation of the WO_3 phase in these samples due to the possible oxidation reaction: $WC + 5/2O_2 \rightarrow WO_3 + CO_2$.

The first exothermic peak, which occurred around 370 °C, is associated with the decomposition temperature of the binder. Therefore, the thermal debinding temperature should be kept below this temperature. Since no dwelling can be performed in DTA/TG experiments, the thermal debinding temperature could not be precisely determined. To verify the optimum conditions, several tests were done and it was found out that temperatures higher than 300 °C would cause oxidation problems after a dwell of 12 h.

Following thermal debinding, to get a general idea about the shrinkage characteristics and thermal analyses, DTA/TG and dilatometer measurements were carried out under argon (Ar) atmosphere. The DTA/TG and dilatometer curves of the thermally debinded 3Y-TZP/40WC composite are given respectively in Fig. 3a and b.

As seen in Fig. 3, the DTA/TG and dilatometer measurements until 1590 °C revealed that even at this temperature, the shrinkage was not completed. Therefore, longer dwelling times were assumed to be required. Furthermore, when DTA/TG observations on thermally debinded extruded samples were examined, for the 3Y-TZP/40WC samples at temperatures higher than 1400 °C, weight increase was observed which can refer to oxidation even under Ar atmosphere. XRD analyses given in Fig. 7 reveal that ZrO_2 and WC phases decomposed at this temperature and new phases such as W_2C, ZrC, W_2Zr and WO_3 oxide phase was formed. For this reason, choosing the proper sintering temperature and atmospheres for the injection molded composites requires a careful evaluation of XRD analyses combined with DT/TG and dilatometer analyses.

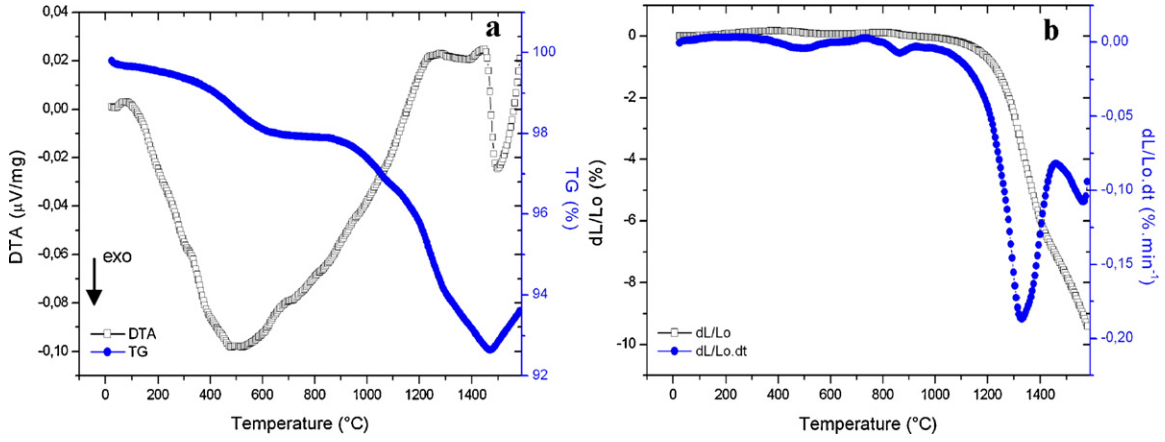

Fig. 3. (a) DTA/TG and (b) dilatometer curves of the thermal debinded 3Y-TZP/40WC composite.

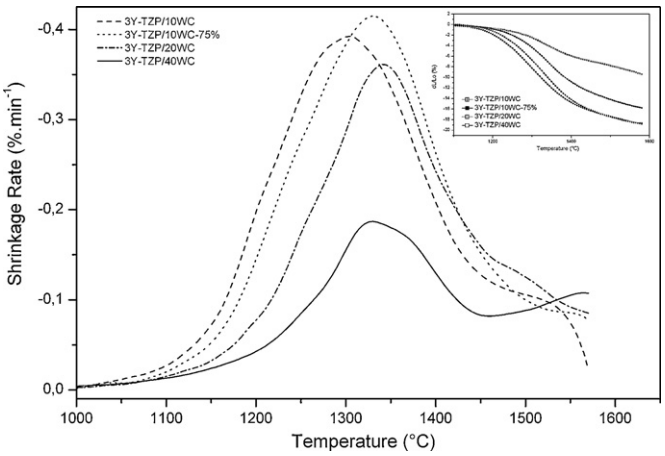

Fig. 4. The shrinkage rate versus temperature graph of the extruded composites.

Shrinkage rates of the composites with different WC amounts as a function of temperature are plotted in Fig. 4.

Fig. 4 reveals that with increasing WC amounts in the matrix, the shrinkage rate decreased. We believe that WC pins the dislocations at the grain boundaries and for this reason excess energy is required for atom movement from the boundary. Therefore, the presence of WC second phase diminished the sintering kinetics. It is clear from the graph that WC fine-particles provided higher diffusion rates and consequently enhanced the shrinkage rate. Sintering was not finalized even at 1550 °C for all the compositions. Therefore, long dwelling times are needed.

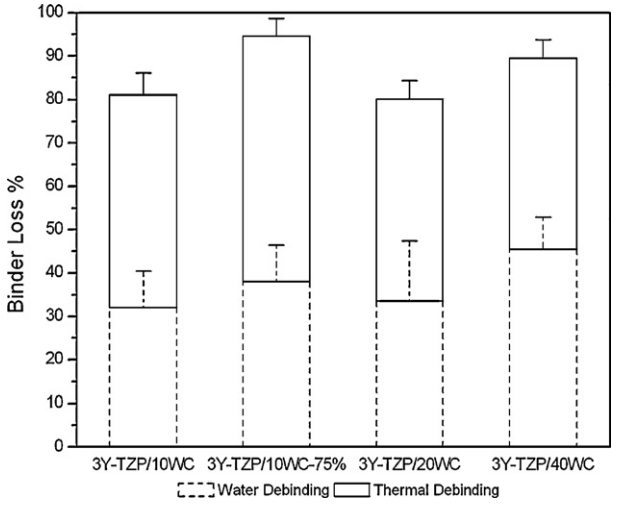

Fig. 5. Percentage binder loss after water and thermal debinding related with the compositions. The binder loss of the plates is represented with the columns and the bars are represented with lines (T).

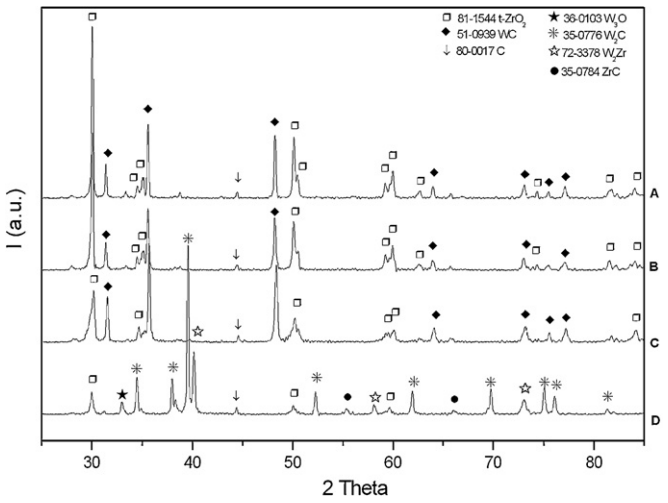

Fig. 7. XRD patterns of the 3Y-TZP/WC composites containing 10 vol.% (A), 10 vol.% (75% coarse) (B), 20 vol.% (C) and 40 vol.% (D) WC sintered at 1550 °C for 6 h.

On the basis of the thermal and mass analyses data obtained by extruded samples given in Figs. 2 and 3, the water and thermal debinding conditions for the injected parts were figured out. The injection molded samples were thermal debinded at 300 °C for 12 h. However, higher temperatures or longer dwelling times caused oxidation. Weight loss was measured in every debinding step. The % binder loss percentage of the plates and bars is shown in Fig. 5.

As seen from Fig. 5, debinded plates lost less binder than the bars due to dimensional differences. The debinding rate was increased as the part became smaller. Likewise, as the parts include smaller particle size, as in the case of the 3Y-TZP/10WC (75% coarse) composite, more binder was removed at the same debinding schedule. After water debinding step, more than 30% of binder was removed in each composition which would further improve thermal debinding. German and Bose [19] claimed that 30% of the binder has to be removed to create an open pore network which is necessary to avoid cracking and blistering during thermal debinding.

Porosimetry results reveal that total open porosity was slightly higher when 25% fine WC particles were used in the 3Y-TZP/10WC composite. On the other hand, smaller pore radius (72 nm) and higher apparent density were obtained with this composition. Lowest porosity was obtained for the 3Y-TZP/20WC composite which had 43 vol.% total open porosity with relatively higher average pore radius. 3Y-TZP/40WC had the largest mean pore radius due to higher amount of WC particles whose mean particle size was larger than that of the 3Y-TZP matrix.

Sintering was carried out at 1550 °C using two different dwelling times with determined stages under controlled atmosphere. Earlier sintering experiments were carried out under Ar atmosphere or in vacuum but in neither of these investigations resulted with sufficient densification although several temperatures and dwelling times were observed. Therefore, attention was paid on the sin-

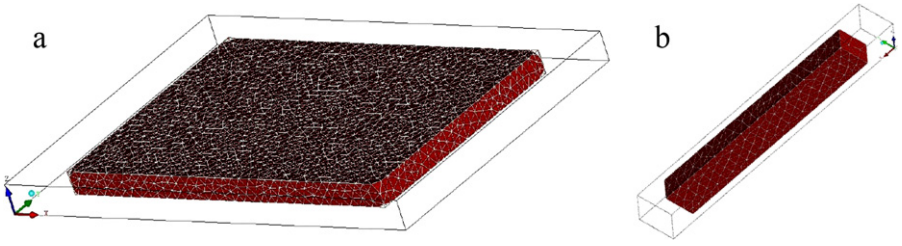

Fig. 6. The shrinkage model of the 3Y-TZP/10WC (a) plates and (b) bars. Debinded and sintered composites are represented as outside rectangle and inside rectangle, respectively.

tering atmosphere to obtain good resultant mechanical properties of the sintered compacts. It was found out that when H_2 gas was used up to a proper temperature followed by flowing Ar gas until the end of sintering, the mechanical properties were significantly improved. However, when sintering was performed at a temperature of 1600 °C higher than 1550 °C, secondary porosity was observed in the microstructure. Haberko et al. [15] also found secondary porosity formation at 1700 °C, which were located close to the carbide grains. They related this formation due to the CO release caused by the reaction between WC and ZrO_2. Therefore, sintering temperature of 1550 °C was chosen as the optimum sintering temperature and higher temperatures were avoided.

Isotropic shrinkage was investigated for the injection molded plates and bars after sintering at 1550 °C for 4 and 6 h. The shrinkage was between 20 and 22% at all directions for the 10 vol.% WC dispersed 3Y-TZP samples. As the WC amount was increased, shrinkage lowered to 17–19% for the 20 vol.% WC, and to 13–15% for the 40 vol.% WC containing composites. WC particles pinned the ZrO_2 grain boundaries therefore it inhibited sintering kinetics of the ZrO_2 matrix [20,21]. The shrinkage amounts were slightly the same at longer dwelling times. The shrinkage model of the 10 vol.% WC dispersed composite is shown in Fig. 6. The outer transparent profile refers to the dimensions of the debinded part, and after sintering it got the dimensions shown with red profile.

Injection molded and sintered 40 vol.% WC dispersed composites which have around 92% relative density, have extremely low hardness and Young's modulus values according to the high porosity level. As mentioned earlier [22], sintering at higher temperatures also did not improve the properties due to secondary pore formation. Additionally, sintering at longer times (longer than 4 h) caused bending and cracking. Hence, the composites with a WC amount more than 20 vol.% should be sintered under pressure at lower sintering temperatures and times, similar to those employed in our previous investigation [10]. Hot pressed 32 and 40 vol.% WC dispersed ZrO_2 matrix composites had 98% and 96% relative density, respectively [10].

On the other hand, if the system had lower amount of the secondary hard phases (less than 40 vol.% WC), the relative densities and mechanical properties were measured to be higher. Measured physical and mechanical properties such as % relative density, Young's modulus, flexural bending strength, Vickers hardness and fracture toughness values of the 10 vol.% and 20 vol.% WC dispersed 3Y-TZP/WC composites sintered at 1550 °C for 4 h and 6 h are given in Table 3.

As seen in Table 3, the 3Y-TZP/10WC composite sintered at 1550 °C for 6 h had the best overall mechanical properties. It is interesting to note that the 3Y-TZP/10WC samples containing 75 vol.% coarse + 25 vol.% fine-WC particles sintered at the dwell times of 4 h and 6 h did not have the best mechanical properties, indicating that fine WC powder did not improve the hardness, strength and fracture toughness of the composites. However, in our previous hot pressing investigation [10], fine-WC addition enhanced the density, strength, hardness and toughness related with the microstructural changes. Thus, following injection molding the presence of dispersed fine-WC particles in the 3Y-TZP matrix did not facilitate sintering but they behaved as inhibitors during the pressureless sintering step. It can be assumed that the fine-WC particles dispersed around the grain boundaries of zirconia and caused reduction in sintering rate. SEM observations would help to clarify this assumption.

3.2. Characterization of as-sintered 3Y-TZP/WC composites

XRD patterns of the sintered 3Y-TZP/WC composites comprising 10 vol.% WC, 10 vol.% WC (75% coarse), 20 vol.% WC and 40 vol.% WC, all sintered at 1550 °C for 6 h are given in Fig. 7. XRD reflections matched the ICDD card values of the t-ZrO_2 (simple tetragonal Bravais lattice, space group: $P42/nmc$) [23] and WC phases (hexagonal Bravais lattice, space group: $P\bar{6}m2$) [24] for the 3Y-TZP/WC composites comprising 10 vol.% WC, 10 vol.% WC (75% coarse WC + 25% fine-WC), 20 vol.% WC (XRD patterns of A, B and C), indicating that no reaction took place between the matrix and the dispersion for WC contents up to and including 20 vol.%. However, when the WC amount increased to 40 vol.% (Fig. 7, pattern D), the microstructure of the sintered composite contains new metastable and stable phases (W_2C, W_2Zr, W_3O, ZrC) which resulted from kinetic reactions between ZrO_2 and WC. The additional C peak (fcc Bravais lattice, $F\bar{4}3m$ space group) [25] at around 45° for every measurement was analyzed because of the background measurement.

Fig. 8 is the SEM micrographs of the indentation traces of the composites sintered at 1550 °C for 4 h (a–c) and 6 h (d–f), revealing crack deflection, crack branching and bridging mechanisms for all samples. These mechanisms enhanced the fracture toughness of the composites.

On the basis of the microstructural observations of Fig. 8, the most prominently increase in fracture toughness of the 3Y-TZP/20WC composite could be a combination of martensitic phase transformation and crack deflection, crack branching and bridging mechanisms. SEM images in Fig. 8c and f reveal that longer sintering times did not have any effect on the grain size of WC particles. Furthermore, the SEM micrographs belonging to the 3Y-TZP/10WC composite having 25% fine + 75% coarse WC dispersion (Fig. 8b and e) indicate that fine WC particles tend to agglomerate which would deteriorate the mechanical properties. Powder agglomerates are often suppressive to the particle packing characteristics, sintering behavior and ensuing properties especially in ceramic systems [26–30]. In the present investigation, it is very likely that the agglomerations of fine WC particles caused high total open porosities which eventually caused density reductions. A similar observation was also concluded by Suri et al. [31] on the effect of agglomerates for a W-based heavy alloy fabricated powder injection molding and sintering. Thus, on the basis of SEM micrographs shown in Fig. 8b and e, the agglomerates were not destroyed sufficiently during feedstock preparation.

Wear performances of the polished injected parts were examined with unlubricated sliding pin-on-disc test machine. The volumetric wear rate (kv) was calculated by using the Archard's Equation [32] expressed as:

$$kv = \frac{V_{\text{wear}}}{F_N \times s}\left(\frac{\text{mm}^3}{\text{N m}}\right) \quad (1)$$

where F_N is the normal load, s is the sliding distance, V_{wear} is the wear volume and kv is the wear rate. The calculated tribological values of the composites up to 20 vol.% WC addition which were sintered using two different dwelling times (4 h and 6 h) are listed in Table 4.

The tribology results indicated that the parts were wear resistant in the unlubricated environment even with long operation conditions under relatively high normal load. Literature values of friction coefficient of ZrO_2 are in a range between 0.4 and 0.9 in the unlubricated wear conditions and this value is 0.9 for the PSZ (partially stabilized zirconia) [33,34]. In a previous study [10], with the same tribology conditions, the friction coefficient and wear rate of the hot pressed 3Y-TZP were measured as 0.68 and 6.06×10^{-8} mm^3/(N m^{-1}), respectively. With WC addition the friction coefficient lowered till 0.39 for hot pressed 3Y-TZP/40WC composites [10].

The friction coefficient values of the injection molded sintered samples were almost similar in every composite, therefore WC amount, dwelling time and bi-modal particle size distribution did

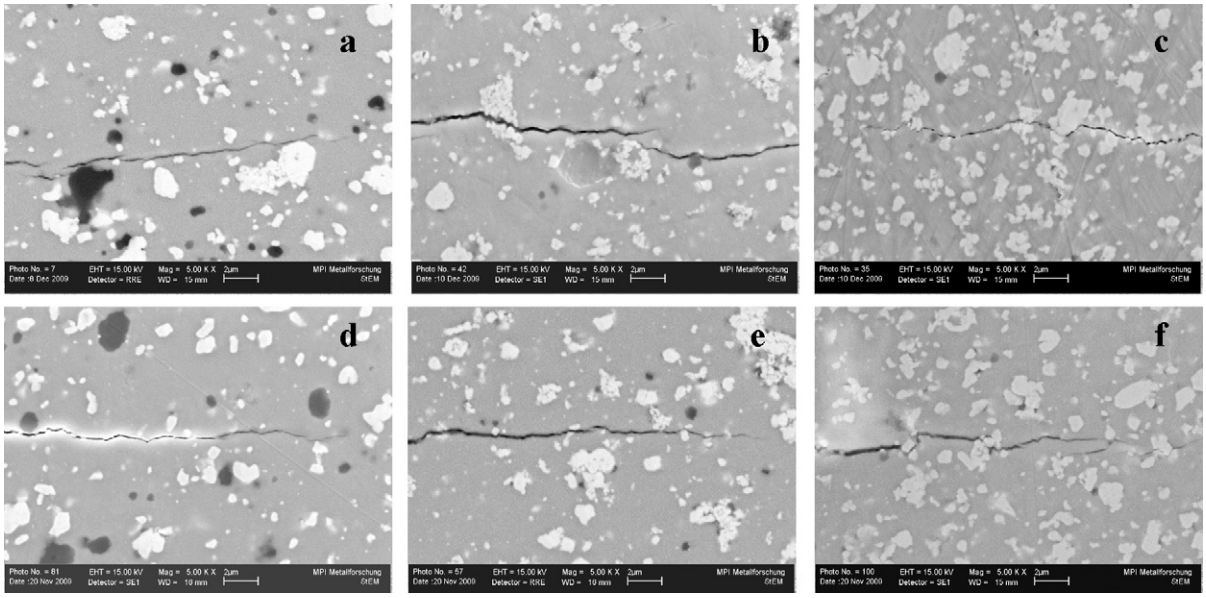

Fig. 8. SEM/BSE images of the crack propagation of the (a) 3Y-TZP/10WC, (b) 3Y-TZP/10WC (75% coarse), (c) 3Y-TZP/20WC composites sintered at 1550 °C for 4 h and (d) 3Y-TZP/10WC, (e) 3Y-TZP/10WC (75% coarse) and (f) 3Y-TZP/20WC composites sintered at 1550 °C for 6 h.

not have much influence on the wear resistance, as expected. The 3Y-TZP/20WC sample which had the highest toughness value of 9.2 MPa $m^{1/2}$ also had the lowest wear amount. With longer dwelling time, the toughness of this composite increased nearly by 59% (Table 3) and this reflected on the wear performance.

The inverted 3D surface topographies of the abraded wear surfaces of the composites are given in Fig. 9. The polished composite surfaces which had roughness values listed in Table 4, worn off between 24 μm and 37 μm deep subsequent to unlubricated reciprocating wear tests under 55 N load and 45 km sliding distance. Homogeneously straight abrasion was obtained all along the wear track in all composites. Comparison of the wear traces shown in Fig. 9d representing 3Y-TZP/10WC composite with those in Fig. 9e representing 3Y-TZP/10WC composite having 25% fine + 75% coarse WC dispersion reveals that the wear resistance was not enhanced as it had for similar composites fabricated by hot-pressing [22]. Similar to the effect on overall densities, the agglomeration of fine WC powders restricted the enhancement of the mechanical properties and that hardness, strength and fracture toughness of the composites were not improved. Therefore, no positive effect of bimodal particle size distribution on mechanical properties could be observed. Higher dwelling time lowered the depth of the abraded surface and the most shallow wear track was obtained for the 3Y-TZP/20WC composite.

Fig. 10a–c is the SEM micrographs of the wear traces belong to the 3Y-TZP matrix reinforced with 10 vol.% WC, 10 vol.% WC (75% coarse particles) and 20 vol.% WC particles, respectively. Additionally surface topography of the 3Y-TZP/10WC composite is given. SEM micrographs represent the middle part of the wear traces obtained after 45 km sliding distance.

SEM images in Fig. 10 indicate that there was neither an adhesion of the debris nor any microcracks along the wear trace. The abraded surfaces were removed away from the debris layer and smooth wear layer remained after a distance of 45 km even at the unlubricated conditions. The bimodal particle size distribution did not have any effect on the surface morphology of the worn surface.

Table 3
Mechanical properties of the 3Y-TZP/WC composites sintered at 1550 °C at the dwell times of 4 h and 6 h.

Composite	Dwell time	% Relative density	$Hv_{0.1}$ (GPa)	E (GPa)	Flexural strength (MPa)	Hv_{10} (GPa)	K_{1C} (MPa $m^{1/2}$)
3Y-TZP/10WC	4 h	99.1	16.4 ± 0.2	287 ± 3	824 ± 96	13.2 ± 0.3	6.3 ± 0.2
	6 h	100.0	16.1 ± 0.3	278 ± 2	1087 ± 112	13.6 ± 0.3	6.2 ± 0.1
3Y-TZP/10WC (75% coarse)	4 h	95.4	13.8 ± 0.5	246 ± 3	568 ± 42	11.3 ± 0.1	6.0 ± 0.1
	6 h	96.9	13.7 ± 0.7	251 ± 2	661 ± 41	11.8 ± 0.4	6.1 ± 0.3
3Y-TZP/20WC	4 h	86.6	10.8 ± 0.4	225 ± 3	305 ± 60	10.0 ± 0.3	5.8 ± 0.5
	6 h	93.4	14.0 ± 0.3	270 ± 2	703 ± 93	11.8 ± 0.1	9.2 ± 0.6

Table 4
Surface roughness (R_a) of the polished surfaces and dry reciprocating wear test results of 3Y-TZP/WC composites under 55 N normal load with a sliding distance (s) of 45 km against WC–Co.

Composite	Dwell time	R_a (μm)	Friction force (N)	Friction coefficient (μ)	Wear volume (mm^3)	kv (10^{-8} $mm^3/(N\,m^{-1})$
3Y-TZP/10WC	4 h	0.003	29.10	0.53	0.06	2.4
	6 h	0.005	31.32	0.57	0.06	2.4
3Y-TZP/10WC (75% coarse)	4 h	0.011	30.59	0.56	0.09	3.6
	6 h	0.004	33.87	0.62	0.06	2.4
3Y-TZP/20WC	4 h	0.008	33.14	0.60	0.14	5.7
	6 h	0.004	31.05	0.56	0.05	2.0

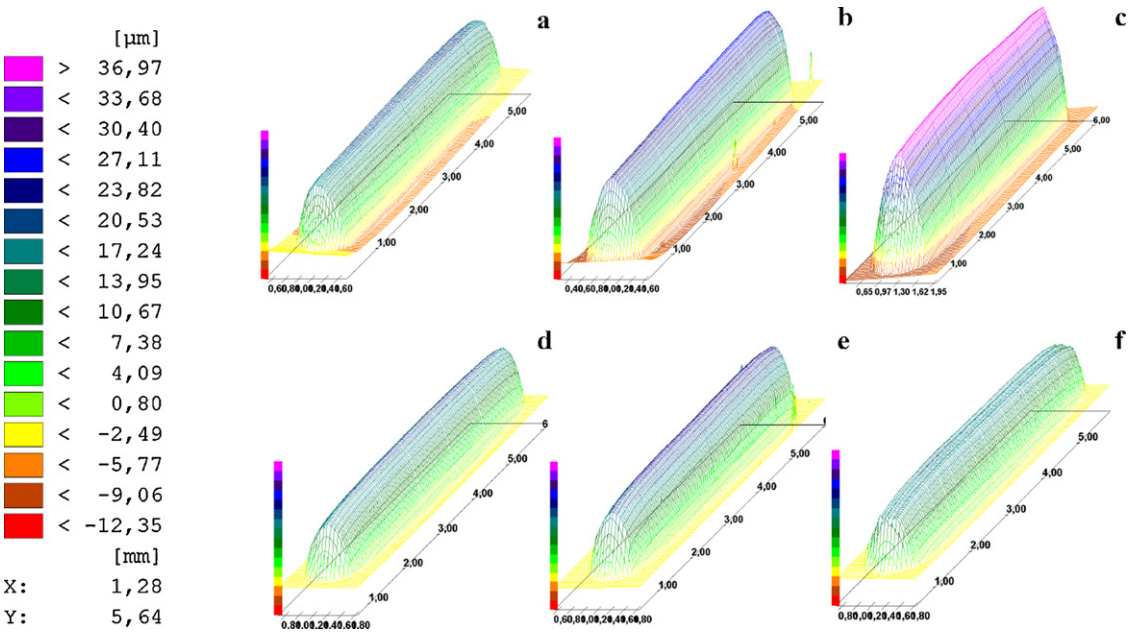

Fig. 9. Inverted 3D surface profiles of the composites subsequent to 45 km unlubricated reciprocating wear test. The tracks belong to 3Y-TZP/10WC (a and d), 3Y-TZP/10WC (75% coarse) (b and e) and 3Y-TZP/20WC (c and f). Sintering at 1550 °C, for 4 h dwell (a–c) and 6 h dwell (d–f).

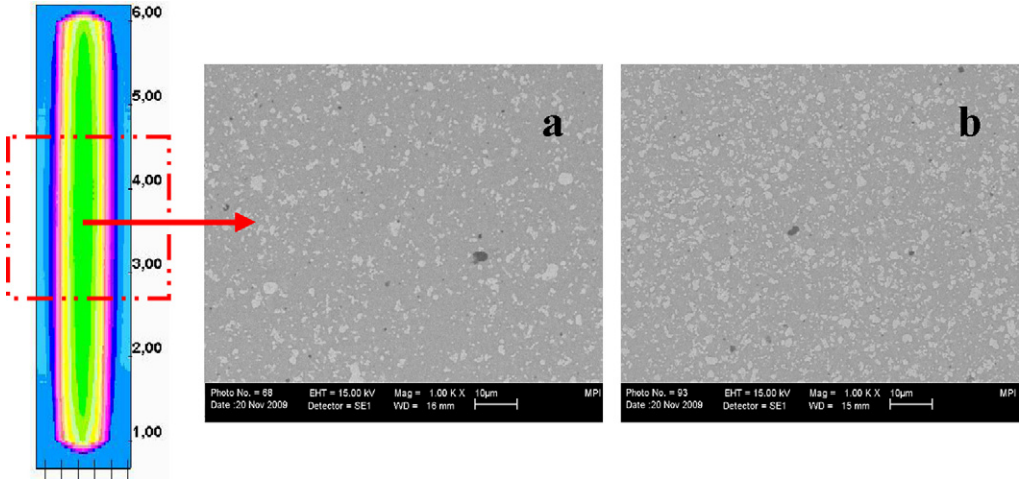

Fig. 10. SEM images taken from in the middle part of the wear traces of composites sintered at 1550 °C for 6 h, 3Y-TZP/10WC (75% coarse) (a), 3Y-TZP/20WC (b); the vertical view of the 3Y-TZP/10WC trace is given as an example on the left.

4. Conclusions

On the basis of the reported results of the present investigation, the following conclusions can be drawn:

1. In general, more than 20 vol.% WC additions to the 3Y-TZP matrix cause problems during processing and sintering. In the injection molding step, higher injection pressures and lower speed were needed for processing of the 3Y-TZP/40WC feedstock which caused further jetting problems resulting poor surface quality. On the other hand, with 20 vol.% WC dispersed feedstock the obtained surface quality was satisfactory.
2. Sintering process was carried out partly in H_2 atmosphere till 1550 °C. At higher sintering temperatures, secondary porosities were observed. Additionally, sintering at longer times caused bending and cracking. Thus, 1550 °C was determined as the optimum sintering temperature for the 3Y-TZP/10WC and 3Y-TZP/20WC composites.
3. Isotropic shrinkage was obtained in all the injection molded parts after sintering at 1550 °C for 4 and 6 h. Mechanical properties varied due to WC addition and dwelling time. Relative density and further mechanical properties enhanced with lower secondary hard phase addition. Highest strength and hardness were obtained with 6 h sintered 3Y-TZP/10WC composite. On the other hand, significant enhancement in fracture toughness was obtained by 3Y-TZP/20WC composite which had 9.2 MPa $m^{1/2}$ toughness. This increase can be attributed to combination of martensitic phase transformation and crack deflection, crack branching and bridging mechanisms. Agglomeration problem of the fine WC powder restricted the enhancement of the mechanical properties of 3Y-TZP/10WC (75% coarse) composite therefore no positive effect of bimodal particle size distribution could be observed.
4. The tribology results indicate that the parts had low wear rate in the unlubricated environment even with long operation conditions under relatively high normal load. The friction coefficient values were almost similar in every composite, there-

fore WC amount, dwelling time and bi-modal WC particle size distribution did not have much influence on the wear resistance.

Acknowledgment

This research was made possible by a research grant provided by Deutscher Akademischer Austausch Dienst (DAAD) and this is gratefully acknowledged.

References

[1] R.V.B. Oliveira, V. Soldi, M.C. Fredel, A.T.N. Pires, Journal of Materials Processing Technology 160 (2) (2005) 213–220.
[2] R. Vaszen, D. Stover, Journal of Materials Processing Technology 92 (93) (1999) 77–84.
[3] D.M. Liu, W.J. Tseng, Ceramics International 24 (6) (1998) 471–481.
[4] G Anné, S. Put, K. Vanmeensel, D. Jiang, J. Vleugels, O. Van der Biest, Journal of the European Ceramic Society 25 (2005) 55–63.
[5] Z. Pedzich, K. Haberko, J. Piekarczyk, M. Faryna, L. Litynska, Materials Letters 36 (1) (1998) 70–75.
[6] D. Jiang, O. Van der Biest, Jef Vleugels, Journal of the European Ceramic Society 27 (2–3) (2007) 1247–1251.
[7] Z. Pedzich, M. Faryna, K. Haberko, in: S. Adali, E. Verijenko (Eds.), Composite Science and Technology, University of Natal, Durban, South Africa, 1996, pp. 379–384.
[8] E. Volceanov, S. Motoc, A.T. Abagiu, A. Volceanov, S. Stoleriu, Journal of the European Ceramic Society 27 (2–3) (2007) 763–768.
[9] J. Vleugels, O. Van der Biest, Journal of the American Ceramic Society 82 (1999) 2717–2720.
[10] N. Ünal, F. Kern, M.L. Övecoglu, R. Gadow, EURO PM2009 Proceedings, vol. 3, 2009, pp. 47–53.
[11] Z. Pedzich, K. Haberko, M. Faryna, J. Kozubowski, The Sixth Conference and Exhibition of the European Ceramic Society, vol. 60, 1999, p. 341.
[12] Z. Pedzich, Journal of the European Ceramic Society 24 (12) (2004) 3427–3430.
[13] S. Salehi, O. Van der Biest, J. Vleugels, Journal of Materials Science 43 (2008) 5784–5789.
[14] S.G. Huang, K. Vanmeensel, O. Van der Biest, J. Vleugels, Journal of the European Ceramic Society 27 (10) (2007) 3269–3275.
[15] K. Haberko, Z. Pedzich, M. Faryna, J. Dutkiewicz, A. Kowal, in: P. Antoni, Tomsia, M. Andreas, Glaeser (Eds.), Ceramic Microstructure: Control at the Atomic Level, Plenum press, NY, 1998.
[16] Z. Pedzich, K. Haberko, Key Engineering Materials 132–136 (1997) 2076–2079.
[17] K. Haberko, Z. Pedzich, G. Rog, M. Bucko, M. Faryna, European Journal of Solid State and Inorganic Chemistry 32 (7–8) (1995) 593–601.
[18] DIN EN ISO 6872, Dental Ceramic, International Organization for standardization, Berlin, 1998, pp. 2–9 (in German).
[19] R.M. German, A. Bose, Injection Molding of Metals and Ceramics, Metal Powder Industries Federation, Princeton, 1997.
[20] E. Lassner, Tungsten: Properties, Chemistry, Technology of the Element, Alloys, and Chemical Compounds, Kluwer Academic/Plenum Publishers, NY, 1999.
[21] Z.J.L. Kang, Sintering: Densification, Grain Growth, and Microstructure, Elsevier Butterworth-Heinemann, Amsterdam, Boston, London, 2005.
[22] N. Ünal, F. Kern, M.L. Öveçoğlu, R. Gadow, Journal of the European Ceramic Society, in preparation.
[23] Powder Diffraction Files, Card No. 81-1544, Database Edition, International Centre for Diffraction Data (ICDD), Newton Square, PA 19073-3273, USA, 2006.
[24] Powder Diffraction Files, Card No. 51-0939, Database Edition, International Centre for Diffraction Data (ICDD), Newton Square, PA 19073-3273, USA, 2006.
[25] Powder Diffraction Files, Card No. 80-0017, Database Edition, International Centre for Diffraction Data (ICDD), Newton Square, PA 19073-3273, USA, 2006.
[26] F.F. Lange, M. Metcalf, Journal of the American Ceramic Society 66 (1983) 398–406.
[27] P. Suri, S.V. Atre, R.M. German, J.P. DeSouza, Materials Science and Engineering A 356 (2003) 337–344.
[28] P. Suri, S.V. Atre, R.M. German, J.P. DeSouza, Powder Metallurgy 47 (2004) 137–143.
[29] J. Cheng, S. Zha, X. Fang, X. Liu, G. Meng, Materials Research Bulletin 37 (2002) 2437–2446.
[30] M. Trunec, P. Dobsak, J. Cihlar, Journal of the European Ceramic Society 20 (2000) 859–866.
[31] P. Suri, R.M. German, J.P. DeSouza, International Journal of Refractory Metals & Hard Materials 27 (2009) 683–687.
[32] J.F. Archard, W. Hirst, Mathematical and Physical Sciences 236 (1206) (1956) 397–410.
[33] E. Richard Booser, Society of Tribologists and Lubrication Engineers, vol. III, 1st ed., CRC press, USA, 1994.
[34] K. Kato, H. Furuyama, M. Mizumoto, Proceeding of Japan Int. Tribology Conf., Nagoya, 1990, pp. 261–266.